Hindawi
Mathematical Problems in Engineering
Volume 2018, Article ID 7859521, 15 pages
https://doi.org/10.1155/2018/7859521

Research Article

An Improved Rollover Index Based on BP Neural Network for Hydropneumatic Suspension Vehicles

Xiaotong Dong,[1] Yi Jiang,[1] Zhou Zhong,[2] Wei Zeng,[2] and Wei Liu[1]

[1]*School of Aerospace Engineering, Beijing Institute of Technology, Beijing, China*
[2]*China Academy of Launch Vehicle Technology, Beijing, China*

Correspondence should be addressed to Yi Jiang; jy2818@163.com

Received 29 September 2017; Revised 6 March 2018; Accepted 15 March 2018; Published 24 April 2018

Academic Editor: Jean-Christophe Ponsart

The 3-DOF rollover model has been established by the Lagrangian second-class equation, taking the road inclination angle, the steering strategy, and the hydropneumatic suspension characteristics into consideration. A 3-layer BP (backpropagation) neural network is applied to predict the road inclination angle and to optimize the rollover model in real-time. The number of the hidden layer neurons for the BP network is also discussed. The numerical calculation of the optimized rollover model is in good agreement with the full-scale vehicle test. Different rollover indexes are compared, and the results indicate that the rollover index of dynamic *LTR* optimized by the BP neural network can evaluate the rollover tendency more accurately in the ramp steering test and the snake steering test. This study provides practical meanings for developing a rollover warning system.

1. Introduction

In recent years, rollover accidents have been comprising a disproportionately large number of highway fatalities [1]. Estimation of the proportion of rollover varies largely from 3.9% [2] to 19% [3], owing to overturning motion which may not be the only event and sometimes is preceded or succeeded by other events such as collision with another vehicle or a fixed object [4]. Nowadays many heavy vehicles are installed with hydropneumatic suspension and heavy vehicles are more prone to rollover than civil cars in certain severe maneuvers. Many mathematical models take suspension travel process simply as springs based on Hooke's law. However, research shows that neglecting the nonlinear characteristics of hydropneumatic suspension is undesirable [5, 6]. Therefore, studying the rollover index of the vehicles with hydropneumatic suspension has a profound significance.

Many researchers have been studying vehicle rollover dynamics, aimed to find the proper rollover index and provide a plausible solution. Andrzej et al. [7] presented the Rollover Prevention Energy Reserve (RPER) function from the perspective of energy transformation. In 1990, Preston-Thomas and Woodroofe [8] built up a rollover control and warning system based on the *LTR* (lateral transfer ratio), a dimensionless normalized value ranging from −1 to 1. *LTR* is defined as the value of the difference between the vertical forces of the left tires and right tires divided by the sum of all vertical tire forces as

$$\mathrm{LTR} = \frac{\sum F_{z,R} - \sum F_{z,L}}{\sum F_{z,R} + \sum F_{z,L}}. \tag{1}$$

Although the tire forces are nonuniformly distributed and difficult to measure in reality, they could be easily reckoned up from the mathematical model. Based on the traditional yaw-roll model, Chen and Peng [9–12] proposed a real-time index called Time-to-Rollover (TTR). Nevertheless, TTR still needs some optimization to proper function at a practical level [13–15]. In addition, Phanomchoeng and Rajamani [16, 17] presented that the LTR based on the 4-DOF model can reliably detect both tripped and untripped rollovers with a 1/8th scaled vehicle test. Hyun and Langari [18] proposed the roll-plane model of the vehicle in conjunction with online vehicle parameter identification and proved that the predicted values of the LTR are close to the simulated results by ArcSim. Woerner et al. [19] used a backpropagation through

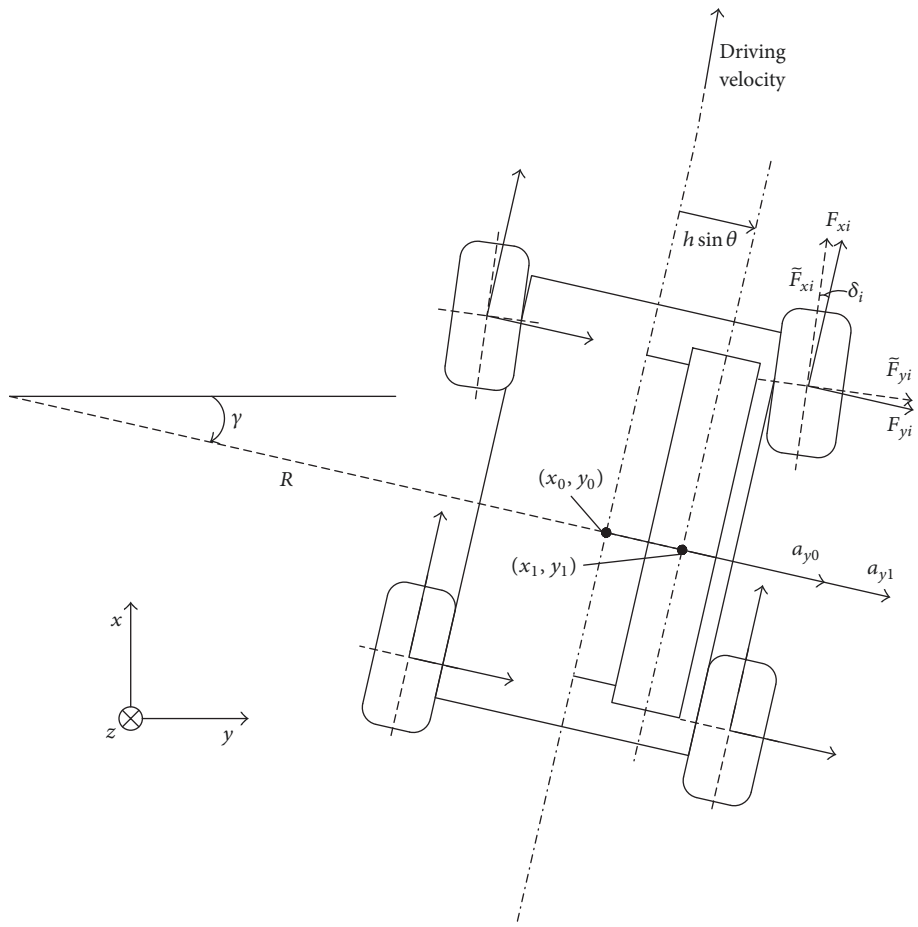

Figure 1: Top view of rollover model in global coordinates.

time algorithm to model and predict the rollover of a tank truck carrying varying liquid volumes. However, the road inclination angle has great influence on the rollover status, which has not been clearly addressed in the study of rollover. As the road inclination angle is difficult to obtain directly, it is necessary to establish the relationship between the road inclination angle and other vehicle dynamic parameters.

As widely employed in the field of machine learning and cognitive science, the artificial neural network is a mathematical computational model network inspired by biological neural networks used to demonstrate the complicated nonlinear relationship [20]. The backpropagation (BP) neural network is a type of the most commonly used neural network with an error backpropagation algorithm that is one of the most popularized and efficient methods for network optimization [21]. By means of the BP neural network, the effect of the road inclination angle could be reflexed in the vehicle rollover dynamics.

The structure of the paper is organized as follows: in Section 2, based on the Lagrangian second-class equation, a vehicle rollover model on the sloping road is established. The nonlinear hydropneumatic suspension characteristics are discussed to deduce the vehicle equivalent stiffness and damping coefficient. An example of the model numerical calculation is analyzed in detail. In Section 3, a BP neural network using a hyperbolic tangent function as the transfer function is applied to optimize the rollover model. Rollover indexes are presented based on the conception of *LTR*. Section 4 begins with a brief introduction on the full-size vehicle test. Then the results of the numerical calculation are discussed and several rollover indexes are put into comparison. Finally, in Section 5, some conclusions are summarized for further studying.

2. Modeling

In this section, a 3-DOF rollover model considering the road inclination angle has been established. The basic assumption is that sprung mass has only roll motion relative to the unsprung mass and the unsprung mass has no pitch motion or roll motion. Notice that to clear the confusion of positive sign and negative sign, all signs of the undeclared values are following the specified coordinate system below.

2.1. Rollover Model Based on Lagrangian Second-Class Equation. The global coordinates are defined as z-axis vertical down to the ground and the yaw angle of the vehicle γ as shown in Figure 1.

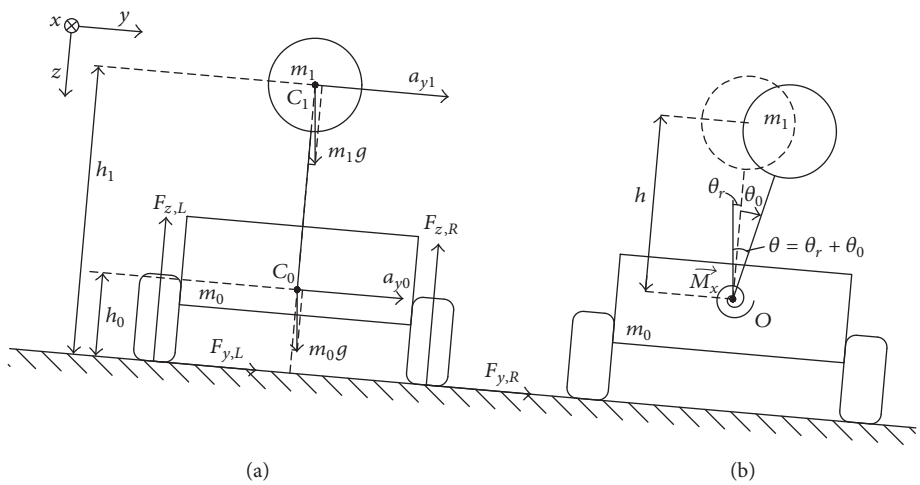

Figure 2: (a) Rear view of rollover model in the specified local coordinates. (b) Internal force and position relationship between sprung mass and unsprung mass.

The positions of the sprung mass m_1 and the unsprung mass m_0 are given as (x_1, y_1) and (x_0, y_0). With the influence of external factors, sprung mass m_1 will slightly roll a small angle θ and change the relative position between m_1 and m_0. Given that the roll radius is h, then the displacement between m_1 and m_0 in xy plane is $h \sin\theta$; then there is

$$\begin{aligned} x_1 &= x_0 - h \sin\theta \sin\gamma, \\ y_1 &= y_0 + h \sin\theta \cos\gamma. \end{aligned} \tag{2}$$

As θ is rather small, there are $\sin\theta \approx \theta$ and $\cos\theta \approx 1$.

And, respectively, the lateral acceleration of m_0 and m_1 is

$$\begin{aligned} a_{y0} &= -\ddot{x}_0 \sin\gamma + \ddot{y}_0 \cos\gamma, \\ a_{y1} &= -\ddot{x}_1 \sin\gamma + \ddot{y}_1 \cos\gamma = a_{y0} + h\left(\ddot{\theta} - \theta\dot{\gamma}^2\right). \end{aligned} \tag{3}$$

The specified local coordinates fixed on the vehicle are defined as x-axis pointing to the vehicle front, y-axis pointing right, and z-axis following the right-hand law, as shown in Figure 2. Figure 2(a) demonstrates the overall force situation for the whole mass while Figure 2(b) shows the internal force and position relationship between sprung mass and unsprung mass.

When the road inclination (or other factors that may induce the unsprung mass to roll) exists as θ_r, it could be reckoned as the ground counterbalancing most of the gravity and the vehicle bearing an extra acceleration $g \sin\theta_r$ in the y direction. It can be seen that the original roll angle θ consists of the road inclination angle θ_r and the relative roll angle θ_0. Road inclination angle θ_r is unknown and by ignoring its changing rate, then there is

$$\begin{aligned} \theta &= \theta_r + \theta_0, \\ \dot{\theta} &= \dot{\theta}_0 \end{aligned} \tag{4}$$

and the total kinetic energy of the system is

$$\begin{aligned} T &= T_0 + T_1 \\ &= \frac{1}{2} m_0 \left(\dot{x}_0^2 + \dot{y}_0^2\right) + \frac{1}{2} m_1 \left(\dot{x}_1^2 + \dot{y}_1^2\right) + \frac{1}{2} J_z \dot{\gamma}^2 \\ &\quad + \frac{1}{2}\left(J_{1,x} + m_1 h^2\right)\dot{\theta}^2, \end{aligned} \tag{5}$$

where J_z is the z moment of inertia of the whole mass, $J_{0,z}$ is the z moment of inertia of the unsprung mass, $J_{1,z}$ is the z moment of inertia of the sprung mass, $J_{0,x}$ is the x moment of inertia of the unsprung mass, $J_{1,x}$ is the x moment of inertia of the sprung mass, $\dot{\gamma}$ is yaw angular velocity ω_z, and $\ddot{\gamma}$ is yaw angular acceleration $\dot{\omega}_z$.

According to the Lagrangian second-class equation, choosing x_0, y_0, θ, γ as the generalized coordinates, then in the global coordinates there is

$$\begin{aligned} &m \cos \ddot{x}_0 - m_1 h \left(\ddot{\theta} \sin\gamma + \dot{\theta} \cos\gamma + \frac{d(\theta\dot{\gamma})}{dt} \cos\gamma \right. \\ &\quad \left. - \theta\dot{\gamma} \sin\gamma\right) = \sum F_x \cos\gamma - \sum F_y \sin\gamma - mg \sin\theta_r \\ &\quad \cdot \sin\gamma, \\ &m \cos \ddot{y}_0 - m_1 h \left(-\ddot{\theta} \cos\gamma + \dot{\theta} \sin\gamma + \frac{d(\theta\dot{\gamma})}{dt} \sin\gamma \right. \\ &\quad \left. + \theta\dot{\gamma} \cos\gamma\right) = \sum F_x \sin\gamma + \sum F_y \cos\gamma + mg \sin\theta_r \\ &\quad \cdot \cos\gamma, \\ &\left(J_{1,x} + 2m_1 h^2\right)\ddot{\theta} + m_1 h \left(-\ddot{x}_0 \sin\gamma + \ddot{y} \cos\gamma\right) \\ &\quad - m_1 h^2 \dot{\gamma}^2 \theta = m_1 g h \sin\theta + M_x, \\ &\left(J_{0,z} + J_{1,z}\right)\ddot{\gamma} = \sum F_{yi} \cdot l_i, \end{aligned} \tag{6}$$

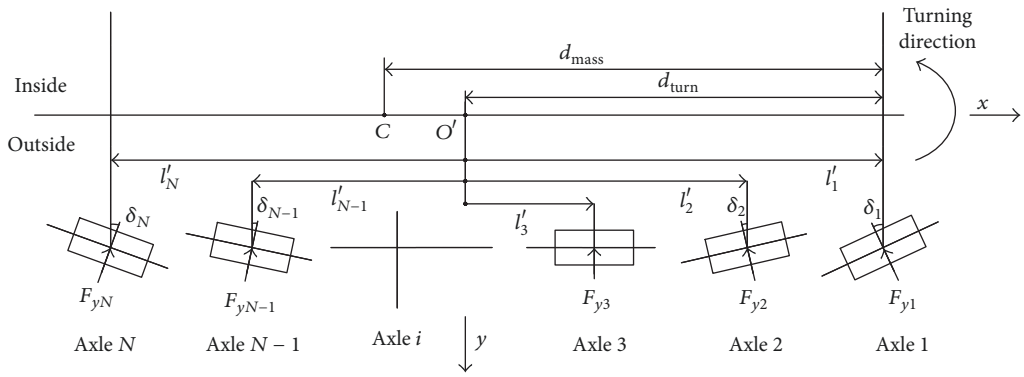

Figure 3: Ackerman steering for multiaxle vehicles.

where M_x is the antiroll moment applied on sprung mass and its calculation will be discussed later in Section 2.2; F_x, F_y are the component forces of one tire in local coordinates; l_i is the distance between axle i and the mass center with positive sign if axle i is ahead of the mass center or negative sign if it is behind the mass center.

In rollover model, researchers are more interested in the vehicle lateral dynamics. Take (3) and (4) into (6) and rewrite it as

$$\begin{aligned} &ma_{y0} + m_1 h\left[\ddot{\theta}_0 - (\theta_r + \theta_0)\,\omega_z^2\right] = \sum F_y + mg\sin\theta_r, \\ &\left(J_{1,x} + 2m_1 h^2\right)\ddot{\theta}_0 + m_1 h a_{y0} - m_1 h^2 \omega_z^2 (\theta_r + \theta_0) \\ &\quad = m_1 gh \sin(\theta_r + \theta_0) + M_x, \\ &(J_{0,z} + J_{1,z})\,\dot{\omega}_z = \sum F_{yi} \cdot l_i. \end{aligned} \tag{7}$$

Equation (7) is the rollover model in the local coordinates. The vehicle's lateral dynamics include circling motion and lateral skid motion, and then there is

$$a_{y0} = \dot{V}_y + \omega_z V_x, \tag{8}$$

where V_y is the lateral velocity of vehicle mass center and V_x is the forward velocity of vehicle mass center. Therefore, the slip angle of tire i is

$$\alpha_i = \arctan\frac{V_y + \omega_z l_i}{V_x - \omega_z B_i} - \delta_i, \tag{9}$$

where B_i is half of the track width, for left tires, $B_i = B$, and for right tires, $B_i = -B$; δ_i is the steering angle of tire i and it is decided by the steering strategy which will be discussed soon.

As for F_{yi}, there is

$$\begin{aligned} F_{yi} &= \widetilde{F}_{yi} \cdot \cos\delta_i = k_t \alpha_i \cdot \cos\delta_i \\ &= k_t \cdot \cos\delta_i \left(\arctan\frac{V_y + \omega_z l_i}{V_x - \omega_z B_i} - \delta_i\right), \quad k_t < 0, \end{aligned} \tag{10}$$

where $\widetilde{F}_{yi}$ is the lateral force of tire i in tire local coordinates and k_t is the tire lateral stiffness.

In order to keep the consistency in the numerical calculation and the test, according to the adopted steering angle measuring instrument for the test, positive steering wheel angle δ_{st} indicates turning left. Therefore, when in left turning scenario, the signs of the steering wheel angle δ_{st} and the roll angle θ are positive and the signs of lateral acceleration a_y and yaw angular velocity ω_z are negative. According to that, all variables are signed, which makes the model calculation standardized. These agreements could clear the confusion caused by different sign declarations.

2.2. Ackerman Steering Strategy. For multiaxle vehicles, which have quite a long chassis and several steering axles, Ackerman steering strategy is commonly applied [22]. Ackerman steering is very suitable for heavy-duty vehicles. One of its principal benefits is to mitigate tire wear, chassis stress, and tire-road additional drag force. The Ackerman steering strategy for multiaxle vehicles can be illustrated in Figure 3. N is defined as the number of axles and $2N$ is the number of tires. Notice that point O' is the turning center of the vehicle and point C is the vehicle mass center. The turning center O' is used to calculate the yaw angular velocity ω_z. These two points are equivalent when the slip angle of mass center keeps at zero.

Applying Ackerman steering strategy, there is

$$\begin{aligned} \frac{l'_i}{\tan\delta_i} &= \frac{l'_j}{\tan\delta_j}, \\ \cot\delta_{i,\text{out}} - \cot\delta_{i,\text{in}} &= \frac{2B}{l'_i}, \end{aligned} \tag{11}$$

where l'_i is the difference of x coordinate between axle i and the turning center O', δ_i is the steering angle of tire i, and $\delta_{i,\text{in}}$ and $\delta_{i,\text{out}}$ are the steering angle of the inner tire and the outer tire for axle i, respectively.

Multiaxle vehicles usually have several steering axles in the front, and some in the rear probably. The unsteering axles do not participate in steering, which means that their steering angle is zero. A new variable q_i is given to indicate which axles are the steering ones and which ones are not. q_i equals one when axle i is a steering axle and equals zero when axle i is

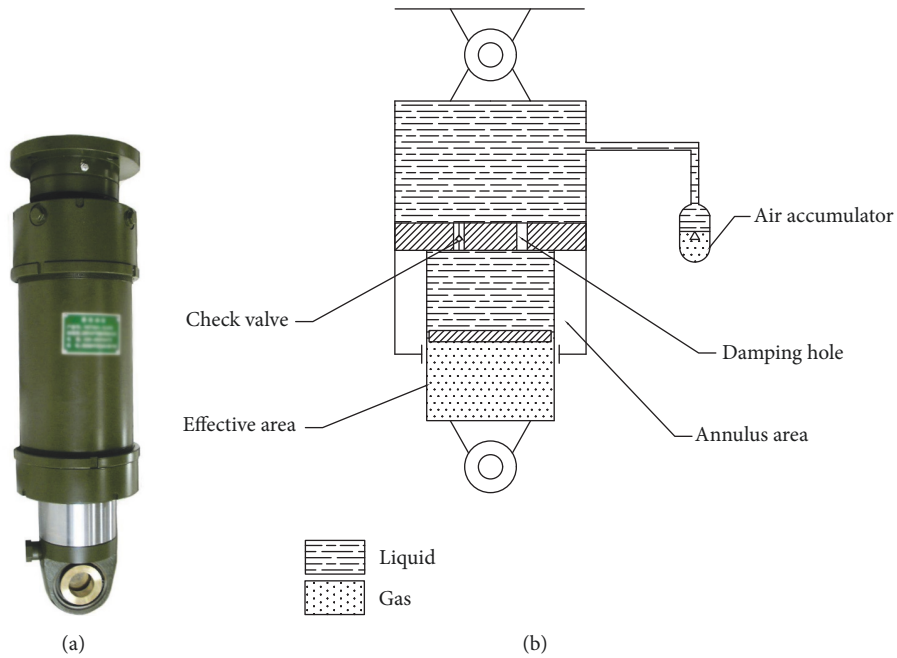

Figure 4: (a) Photo of hydropneumatic spring for vehicle suspension. (b) Structure of one typical kind of hydropneumatic spring.

not. When the linear ratio between the steering angle and $\delta_{1,\text{in}}$ is given as $C_{\delta 1}$, then there is

$$\begin{aligned} \delta_{1,\text{in}} &= C_{\delta 1}\delta_{\text{st}}, \\ \delta_{1,\text{out}} &= \operatorname{arccot}\left(\cot\delta_{1,\text{in}} + \frac{2B}{l_1'}\right), \\ \delta_{i,\text{in}} &= \arctan\left(\frac{l_i'}{l_1'}\tan\delta_{1,\text{in}}\right)\cdot q_i, \\ \delta_{i,\text{out}} &= \arctan\left(\frac{l_i'}{l_1'}\tan\delta_{1,\text{out}}\right)\cdot q_i, \end{aligned} \tag{12}$$

where $q_{1,2,3} = 1$ and $q_{4,5,6} = 0$. When the steering angle δ_i of each tire is obtained the lateral force of each tire could be calculated according to (10). The main parameters of the test vehicle are given in Table 1.

Table 1: Main parameters of the test vehicle (WS-2900).

Parameter	Value	Unit
N	6	-
m_1	55000	kg
m_0	15000	kg
J_x	$6.06e+04$	kg·m^2
J_z	$7.66e+05$	kg·m^2
h	1.2	m
B	1.4	m
H	1.92	m
g	9.8	kg·m/s^2
k (constant)	$3.0e+06$	N/rad
c (constant)	$2.0e+04$	N·s/rad
k_t	4720	N/deg

2.3. Hydropneumatic Suspension. Hydropneumatic suspensions are different from the conventional suspension. The highlight features are compactness, easy installation, and, most importantly, extra heavy payload. Difficult manufacture and high maintenance demands are its major drawbacks. Figure 4(a) demonstrates a common type of hydropneumatic spring for heavy-duty vehicle suspensions. They utilize inert gas as the elastic medium and oil liquid as a support and damping medium, which combines elastic energy storage and damping energy storage into one function unit as seen in Figure 4(b).

It is assumed that the suspension forces on the sprung mass act parallel to the sprung mass z-axis. The elastic force of the hydropneumatic suspension is mainly generated by the piston pushing the liquid to compress the gas in the air accumulator; therefore it shows obvious nonlinear characteristics. According to ideal gas state equation, the change of the gas state during the vehicle suspension vibration can be regarded as an adiabatic process, where the gas polytropic exponent $r = 1.4$. Then the dynamic pressure is [23–25]

$$P_s = \frac{P_p V_p^r}{\left(V_p + A_p \Delta z\right)^r} = P_p\left(1 + \frac{\Delta z}{z_p}\right)^{-r}, \tag{13}$$

where P_p is the balanced pressure; V_p is the balanced air volume; A_p is the effective area of supporting effect; z_p is the balanced deformation of the hydropneumatic spring; Δz is the deformation of the hydropneumatic spring; extension scenario provides $\Delta z > 0$ and compression scenario provides $\Delta z < 0$.

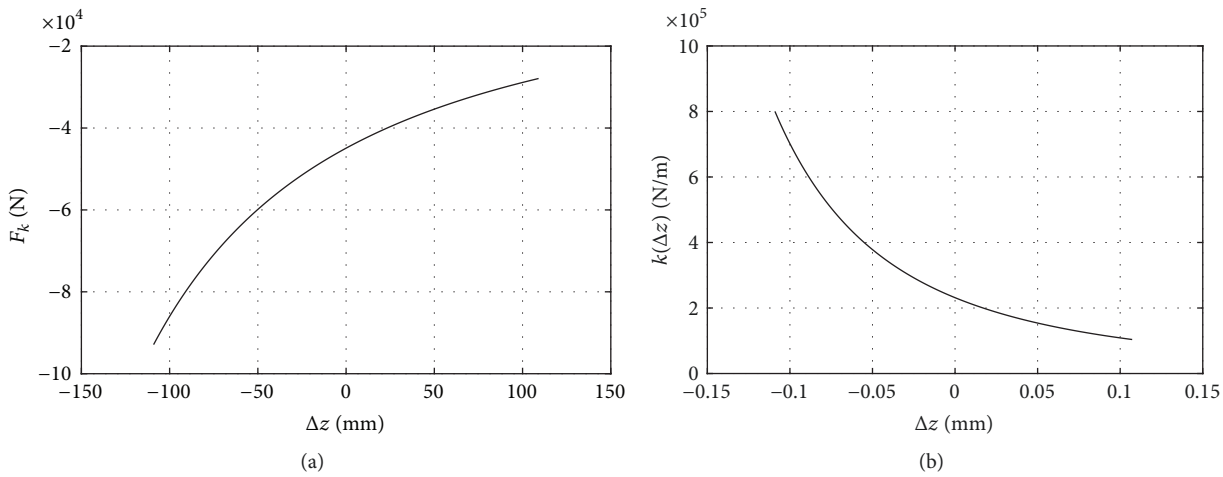

Figure 5: (a) Elastic force versus deformation of one hydropneumatic spring. (b) Stiffness versus deformation of one hydropneumatic spring.

Therefore, according to the specified coordinates, the support force applied on the spring on is written as

$$F_k = -P_s A_p = -P_p A_p \left(1 + \frac{\Delta z}{z_p}\right)^{-r}. \tag{14}$$

It can be seen that the stiffness of hydropneumatic spring becomes larger if it is being compressed and vice versa, as shown in Figure 5. This agrees with the compressibility law of ideal gas.

When the hydropneumatic spring is in the extension scenario, the damping force is generated only by the throttling effect of the damping hole; when in the compression scenario, the damping force is generated by the damping hole and check valve together. Therefore, the damping force of one hydropneumatic spring could be written as [26]

$$\begin{aligned} F_c = {} & \operatorname{sgn}(\Delta\dot{z}) \frac{\rho A_a^3 \Delta\dot{z}^2}{2} \left(C_d A_d + \frac{1}{2} C_c A_c \right. \\ & \left. - \frac{1}{2} \operatorname{sgn}(\Delta\dot{z}) C_c A_c\right)^{-2}, \end{aligned} \tag{15}$$

where $\Delta\dot{z}$ is the velocity of the hydropneumatic spring deformation; ρ is the density of the oil liquid; A_a, C_c, A_c, C_d, and A_d are the dimensional parameters of the hydropneumatic spring. And the sign function is defined as

$$\begin{aligned} &\operatorname{sgn}(\Delta\dot{z}) = 1 \quad \text{extension} \quad (\Delta\dot{z} > 0) \\ &\operatorname{sgn}(\Delta\dot{z}) = -1 \quad \text{compression} \quad (\Delta\dot{z} < 0). \end{aligned} \tag{16}$$

Figure 6 demonstrates the nonlinear damping characteristics of one hydropneumatic spring. As it can be seen, the damping force increases rapidly in compression scenario but very slowly in extension scenario. It also shows that the damping coefficient is linearly related to the deformation velocity, but it is obviously larger in the compression scenario. This means that the damping influence of hydropneumatic spring mainly functions in the extension scenario.

When the roll movement of sprung mass agrees with the assumption in Figure 2(b), the deformations of one couple of hydropneumatic springs installed left and right on the vehicle are equal. Therefore, the roll angle θ_0 can be derived as

$$\theta_0 = \frac{\Delta z}{T}, \tag{17}$$

where T is the distance between the supporting points of hydropneumatic springs and the vehicle symmetry plane.

After the relationship between the roll angle and the deformation of hydropneumatic springs is built, the x moment applied on sprung mass includes two parts: one part caused by suspension stiffness is

$$\begin{aligned} M_{\theta_0} &= N \cdot T \left(F_{k,R} - F_{k,L}\right) \\ &= N \cdot P_p A_p T \left[\left(1 + \frac{T\theta_0}{z_p}\right)^{-r} - \left(1 - \frac{T\theta_0}{z_p}\right)^{-r}\right]; \end{aligned} \tag{18}$$

the other part caused by damping is

$$\begin{aligned} M_{\dot{\theta}_0} &= N \cdot T \left(F_{c,R} - F_{c,L}\right) \\ &= -\operatorname{sgn}\left(\dot{\theta}_0\right) N \\ &\quad \cdot T \frac{\rho A_a^3 \left(T\dot{\theta}_0\right)^2}{2} \left(\left(C_d A_d + C_c A_c\right)^{-2} + \left(C_d A_d\right)^{-2}\right). \end{aligned} \tag{19}$$

In summary, the roll moment yielded by the suspension is

$$M_x = M_{\theta_0} + M_{\dot{\theta}_0}. \tag{20}$$

In the linear model, there is

$$M_x = -k\theta_0 - c\dot{\theta}_0, \quad k, c \text{ is constant.} \tag{21}$$

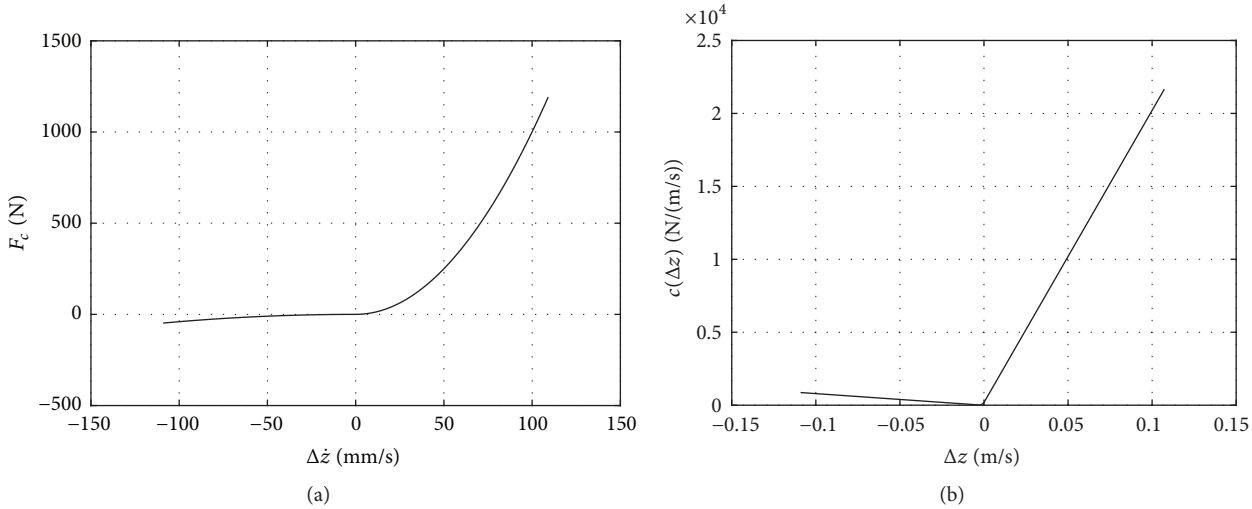

Figure 6: (a) Damping force versus deformation velocity of one hydropneumatic spring. (b) Damping coefficient versus deformation velocity of one hydropneumatic spring.

If comparing (20) with (21), we can also find out that k and c are no longer constant and they are given as

$$k(\theta_0) = -\frac{M_{\theta_0}}{d\theta_0} = N \cdot P_p A_p \frac{T^2}{z_p} \cdot r\left[\left(1+\frac{T\theta_0}{z_p}\right)^{-r-1} + \left(1-\frac{T\theta_0}{z_p}\right)^{-r-1}\right],$$
$$c(\dot{\theta}_0) = -\frac{M_{\dot{\theta}_0}}{d\dot{\theta}_0} = \dot{\theta}_0 \cdot \operatorname{sign}(\dot{\theta}_0) \cdot \left[N\rho A_a^3 T^3 \left((C_d A_d + C_c A_c)^{-2} + (C_d A_d)^{-2}\right)\right]. \quad (22)$$

It can be seen in Figure 7 that the equivalent stiffness of the suspension increases rapidly as the roll angle increases and the equivalent damping of the suspension is linearly related to the roll angle changing rate.

Figure 8 shows how the nonlinear stiffness and damping affect the dynamic response of the roll angle. The stiffness k greatly affects the roll angle static value. And the damping c affects the response time of the roll angle and also causes some steady-state fluctuations. This suggests that the influence of suspension characteristics on the dynamic response of the roll angle is critical. The main parameters of the hydropneumatic suspension are listed in Table 2.

2.4. Model Numerical Calculation: An Example. Assuming that driving speed is constant 6 m/s, the steering wheel input angle and the given road inclination are shown in Figure 9(a). The steering wheel angle is 0° before $t = 10$ s; then it rises to 600° between 10 and 13 seconds; then it remains constant. And at $t = 25$ s it begins to drops to 100° and remains unchanged for the rest time. As to the road inclination, it begins to grow at $t = 5$ s and then stays at about 2.9° until $t = 20$ s that it drops to −1.4° and with some slight fluctuates all the way.

Table 2: Hydropneumatic suspension parameters.

Parameter	Value	Unit
N	6	-
T	0.96	m
ρ	865	kg/m^2
z_p	0.253	m
A_p	$7.9e-03$	m^2
A_c	$7.854e-05$	m^2
A_d	$1.964e-05$	m^2
C_c	0.68	-
C_d	0.68	-
A_a	$3.5e-03$	m^2

For the sake of comparing and analyzing, the working time is divided into five time periods as shown below:

(A) $t = 0$~5 s: no steering angle; no road inclination angle

(B) $t = 5$~10 s: no steering angle; road inclination angle increases

(C) $t = 10$~20 s: steering angle increasing then unchanging; road inclination angle staying top value (around 2.9°)

(D) $t = 20$~25 s: steering angle unchanging then decreasing; road inclination dropping to bottom value (around −1.4°)

(E) $t = 25$~40 s: steering angle staying at 100°; road inclination angle oscillating very slightly.

These five time periods could represent a typical ramp steering case with the influence of road inclination. To validate the

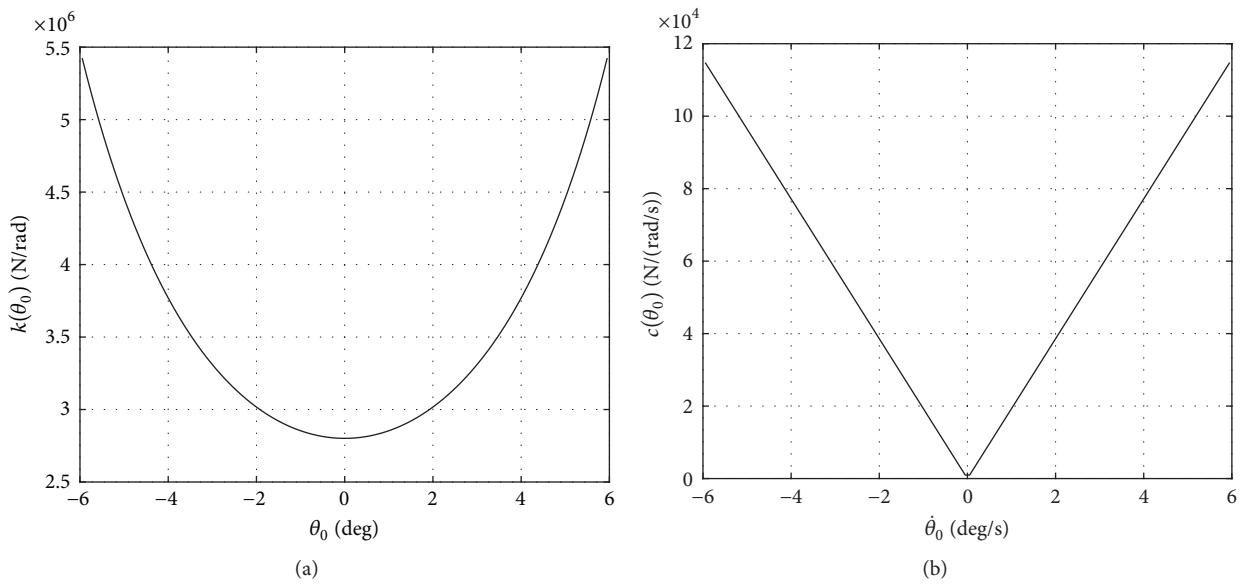

Figure 7: (a) Equivalent stiffness of suspension. (b) Equivalent damping of suspension.

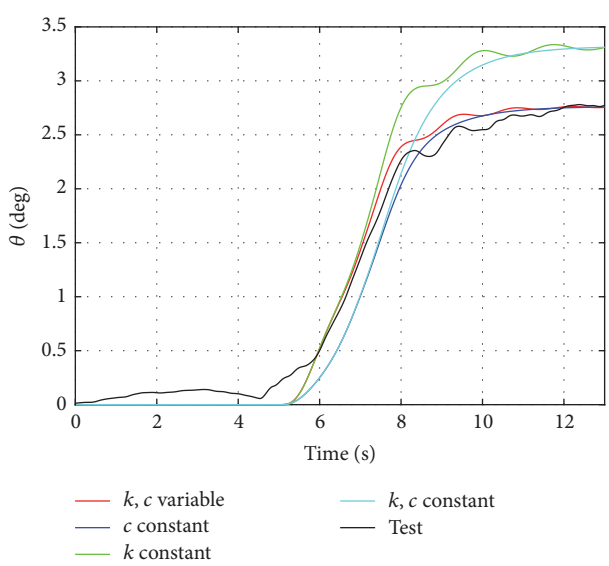

Figure 8: Dynamic response of roll angle with different k and c of suspension.

model, the results need to be thoroughly discussed. Analysis of the roll angle results shown in Figure 9(b) is given below:

(A) As there is no steering angle and no road inclination angle, θ_0 and θ are both zero.

(B) As road inclination angle increases with no steering angle, θ_0 goes along with θ_r.

(C) As road inclination angle stays unchanged and the steering angle begins to increase, θ_0 follows the flat road ramp steering case, which means that θ_0 changes with the steering angle. If steering angle is positive, θ_0 gets bigger; if it is negative, θ_0 gets smaller. In this case, θ_0 is about 3.5° at $t = 18$ s.

(D) At $t = 20$ s, θ_r drops to the bottom quickly, which means that θ_0 should drop too. However, the dropping magnitude of θ_0 should less than that of θ_r because the positive steering angle is trying to keep θ_0 positive. At $t = 23$ s, θ_0 is about 2.6° and θ is 1.13°. Apparently, the steering angle is dominating in this time period.

(E) Finally, the steering angle decreases to a small positive value with a negative road inclination value. At $t = 36$ s, θ_0 is around 0.08° and θ is around −1.39°; the road inclination is dominating the roll angle now.

In conclusion, the roll angle is influenced by the coupling effect between the steering angle and the road inclination angle, which means that its value is dominated by the steering angle when the steering angle is big enough; otherwise it is dominated by the road inclination angle instead. What is more, this relationship is difficult to predict. Therefore, a neural network is applied to establish the relationship between them.

3. Neural Network Model

3.1. BP Neural Network Modeling. The BP neural network has the characteristics of propagating the errors backward through the network after the signal forward propagation, by computing the gradient for each synaptic link and nodal bias using the chain rule, which has the powerful capacity for nonlinear mapping to reveal the internal law of the experimental data. A typical BP neural network structure is given in Figure 10.

The forward propagation of the hidden layer and the output layer can be expressed as

$$o_{kj} = f_j\left(\sum_i w_{ij} o_{ki}\right), \tag{23}$$

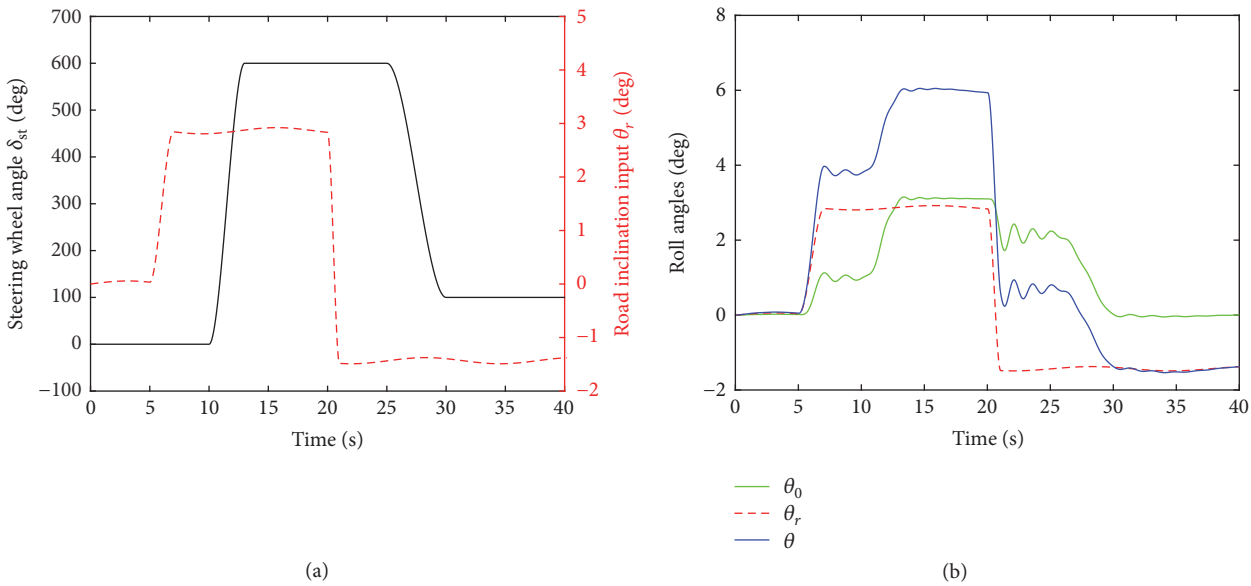

FIGURE 9: (a) Input parameters of the model. (b) Calculation result of roll angles.

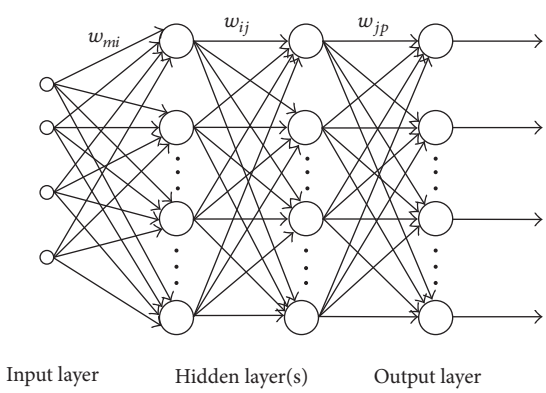

FIGURE 10: Typical BP neural network structure.

where f_j is the jth transfer function. w_{ij} is the connection weight, which represents the weight for the neurons i in the previous layer relative to the neurons j in the current layer. o_{kj} and o_{ki} are the outputs of the neurons i in the previous layer and the neurons j in the current layer for training sample k, respectively.

In this case, the transfer function is the hyperbolic tangent function, given in

$$f(u) = \tanh(u) \tag{24}$$

and with

$$f'(u) = 1 - f^2(u). \tag{25}$$

The training error gradient for the output layer is expressed as

$$\delta_{kj} = \left(1 - o_{kj}^2\right)\left(d_{kj} - o_{kj}\right), \tag{26}$$

where δ_{kj} and d_{kj} are the training error gradient and the target value for the neurons j in the output layer for training sample k, respectively.

The training error gradient for the hidden layer is expressed as

$$\delta_{kj} = \left(1 - o_{kj}^2\right)\sum_m \delta_{km} w_{mj}. \tag{27}$$

In the current iteration step n, the weights are updated according to

$$\Delta w_{ji}(n) = \eta_{BP}\delta_{kj}(n)\, o_{kj}(n) + \alpha_{BP}\Delta w_{ji}(n-1), \tag{28}$$

where η_{BP} is the learning rate of BP network, α_{BP} is a momentum term, which could adjust the amount of corrections and avoid the local minimum [27].

Therefore, the new weights are updated as below

$$w_{ji}(n+1) = w_{ji}(n) + \Delta w_{ji}(n). \tag{29}$$

The initial weights of BP network are regarding the solutions, and usually they are initialized to small values between −1 and 1.

The traditional method of rollover model calculation is to take the driving velocity V_x and the steering wheel angle δ_{st} as the inputs, regardless of the road inclination angle. The schematic of the cooperating process of the rollover model and BP neural network is shown in Figure 11. The BP network in this case has one hidden layer. The driving velocity v_x, steering wheel angle δ_{st}, and total roll angles θ are given as the network 3 inputs and the road inclination angle θ_r is the target output. Resorting to the trained neural network, the road inclination angle could be predicted and applied to the rollover model in real-time. And the rollover index, LTR, could be updated according to the optimized results from the BP network.

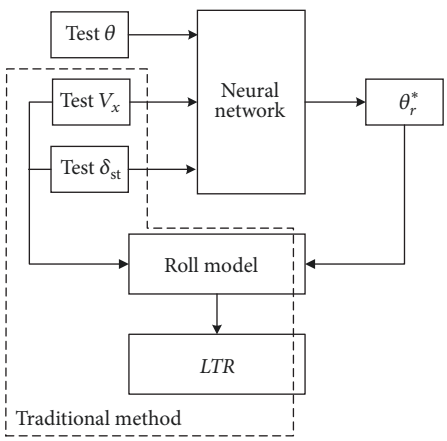

FIGURE 11: Schematic of the cooperating process of the rollover model and BP neural network 8.

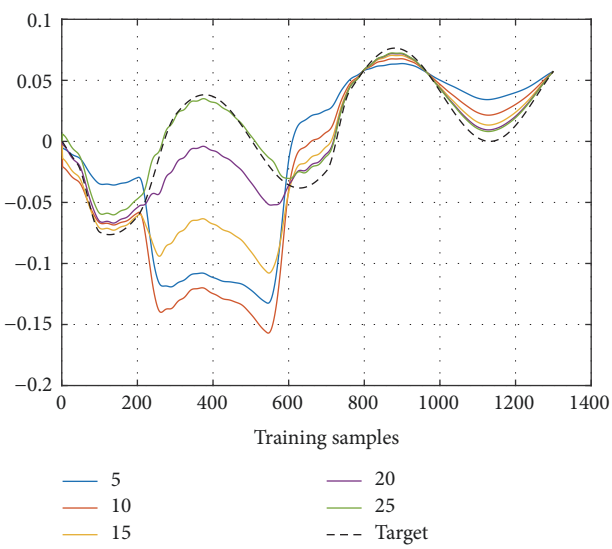

FIGURE 12: Iterations of BP NN of eight hidden neurons.

3.2. Neural Network Training. To train the BP neural network, we need to obtain enough training samples and test samples from the established rollover mathematical model. In the design of the sample data, try to keep the diversity of inputs and reduce the repetition. And normalize all the training samples and keep the target output in the $(-1, 1)$ interval, which is due to the hyperbolic tangent function chosen to be the transfer function.

The total number of training samples is 6500 and the number of test samples is 1300. In training processing, random sample selection is encouraged because it conduces to the weight space search with randomness and avoids the local minimum to a certain extent. As it can be seen in Figure 12, when the number of hidden neurons is 8 and the BP neural network is iterated after 5, 10, 15, 20, and 25 times, respectively, the neural network is approaching the target output gradually, which meets the convergence requirements.

To select the number of hidden neurons, several neural networks of different hidden neurons are put into training;

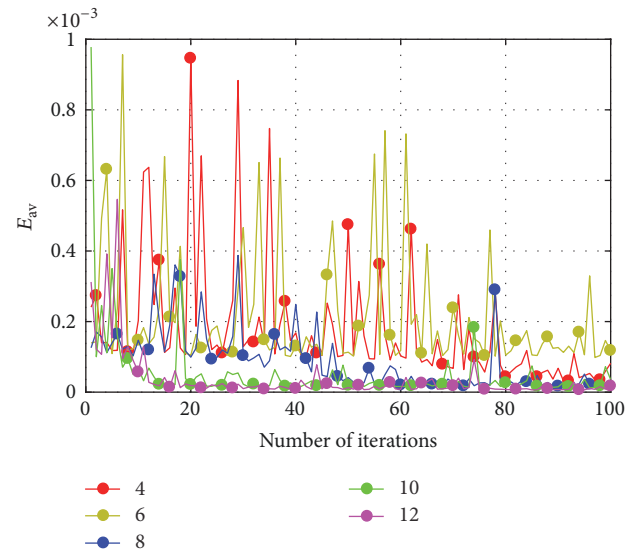

FIGURE 13: Iterations of the average value of error using different hidden neuron numbers.

the results are shown in Figure 13. When the number of hidden neurons s is less than or equal to 8, the average value of error E_{av} is still large after iteration 100 times. When the number of hidden cells is bigger than 10 or more, the average value of error E_{av} of the network can reach $1e-4$ after 20 iterations and basically meet the convergence requirements. Therefore, we choose 10 as the final number of hidden neurons for the BP network. It is efficient and can meet the convergence requirements fast.

3.3. Rollover Indexes. With the assumption that roll dynamic performance of suspension can be ignored, the static lateral *LTR* is given as [28]

$$\mathrm{LTR}_s = -\frac{a_{y1}H}{gB}, \tag{30}$$

where H is the vehicle mass center height.

The dynamic *LTR* (normalized load transfer) is calculated by [29–32]

$$\mathrm{LTR}_d = \frac{k(\theta_0)\theta}{mgB}. \tag{31}$$

According to the rollover model and the BP network built in the previous section, the two new rollover indexes optimized by BP network can be written as

$$\begin{aligned} \mathrm{LTR}_s(\mathrm{NN}) &= -\frac{a_{y1}^* H}{gB}, \\ \mathrm{LTR}_d(\mathrm{NN}) &= \frac{k(\theta_0^*)\theta^*}{mgB}. \end{aligned} \tag{32}$$

The sign "$*$" stands for results from the BP network. Therefore, four rollover indexes, including LTR_s, LTR_d, $\mathrm{LTR}_s(\mathrm{NN})$, and $\mathrm{LTR}_d(\mathrm{NN})$, would be put into the comparison.

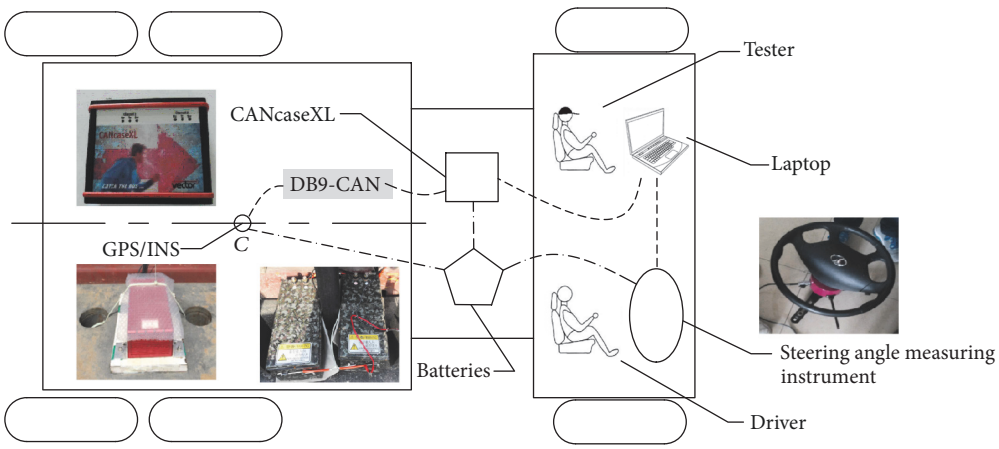

Figure 14: Layout and staffing arrangement of the experiment.

4. Results

4.1. Full-Size Vehicle Test. The vehicle experiment took place in a broad area; no winds affected the experiment and the driver is experienced. However, there were some limits of experiment time and the evenness of road surface could not be guaranteed. As we had some concerns about only gyros and accelerometers are not accurate enough for dynamic measuring condition, this experiment resorted to GPS (Global Positioning System)/INS (Inertial Navigation System) devices. Combining GNSS (Global Navigation Satellites System) receivers, an inertial measurement unit, an internal storage, and a real-time onboard processor all in one integrated unit, the GPS/INS devices can deliver position, velocity, and orientation measurements accurately. The settlement of the measuring devices and staffing arrangement is illustrated in Figure 14.

A steering angle measuring instrument was set on the steering wheel and the driver was made sure to be comfortable with it. The data record CANcaseXL and batteries were fixed on the car frame in behind the cab. The GPS/INS device was installed right above the mass center, on the top of the payload and the centerline of vehicle symmetrical surface. The devices transmit data through CAN bus to data recorder CANcaseXL, then to the laptop finally. The laptop also received information from steering angle measuring instrument; the experimenter sitting next to the driver is responsible for monitoring the devices and the collecting data during the experiment.

In the practice for test purpose, keeping the vehicle at a steady driving velocity was quite challenging. In addition, it was very confusing for the driver to balance between the experiment requests and one's own judgements. Therefore, the driver must take enough test drives before the driving test starts.

4.2. Test Results

4.2.1. Ramp Test. In the ramp test, the steering wheel angle grows slowly until the time reaches 27 s, and then it begins to increase rapidly and finally stops when the time is 29 s; then finally it remains at 633° approximately. The forward velocity oscillates around 5.1 m/s. The results of a_{y0}, a_{y1}, and ω_z basically agree with test data as shown in Figure 15 but are slightly ahead of time relative to the test data. It can also be seen that the test ω_z is smooth while the test a_y has many fluctuations. Numerical calculation shows that the difference between a_{y0} and a_{y1} is rather small but the magnitude of a_{y1} varies more violently a_{y0} than at some certain moments.

As it can be seen in Figure 16, the test vehicle has already tilted to the right a little before the steering. At $t = 20\sim25$ s, θ_r is 0.6° approximately. θ without NN is still below zero at this period. And it is quite smaller than the test roll angle in overall test. As to θ with NN, it is bigger than θ without NN because of the effect of road inclination angle θ_r, which is predicted by the BP neural network dynamically. Therefore, the optimized θ with NN performs well in the ramp test in general.

Four different LTR curves are shown in Figure 17. The difference between LTR_s and $\mathrm{LTR}_s(\mathrm{NN})$ is very small but $\mathrm{LTR}_d(\mathrm{NN})$ differs from LTR_d a lot. When $20\,\mathrm{s} < t < 25\,\mathrm{s}$, the vehicle is tilting to right slightly and only $\mathrm{LTR}_d(\mathrm{NN})$ has positive values around P1. Moreover, only $\mathrm{LTR}_d(\mathrm{NN})$ is able to indicate the most dangerous moment and at P2 acutely.

4.2.2. Snake Test. In snake test, the steering angle changes with time and the maximum value is about 300°. The forward velocity fluctuates from 9.7 to 10.1 m/s. And there are obvious road inclinations in the test field where the long test road surface is high in the middle and low on both sides for drainage purpose. As can be seen in Figure 18, the numerical calculation results of a_{y0}, a_{y1}, and ω_z are bigger than the results of snake test, especially when the steering wheel angle is small relatively. But overall, the curves coincide with the test results. Similar to the ramp test, both of them have the same changing trend and the magnitude of a_{y1} is slightly bigger than a_{y0}.

It can be seen that the test roll angle is strongly asymmetrical in Figure 19. The max value is up to 4.8° at $t = 25$ s and the min value is only −1.8°. Similar to the ramp test, θ_0 with

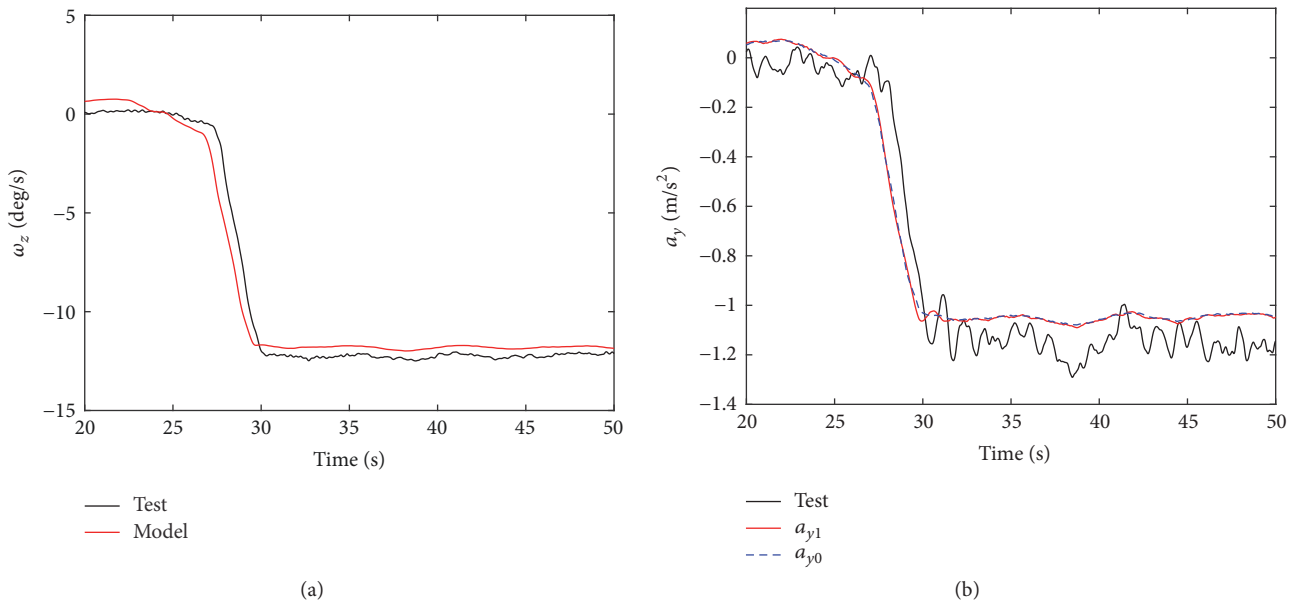

Figure 15: Results of numerical calculation in ramp test.

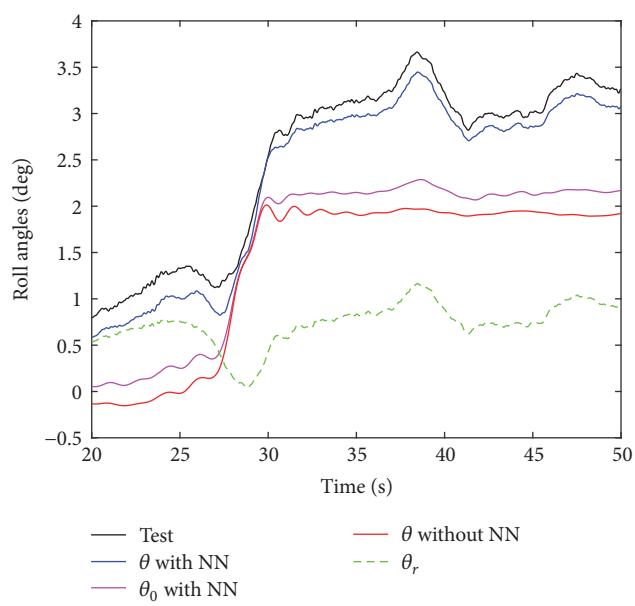

Figure 16: Comparison of different roll angles in ramp test.

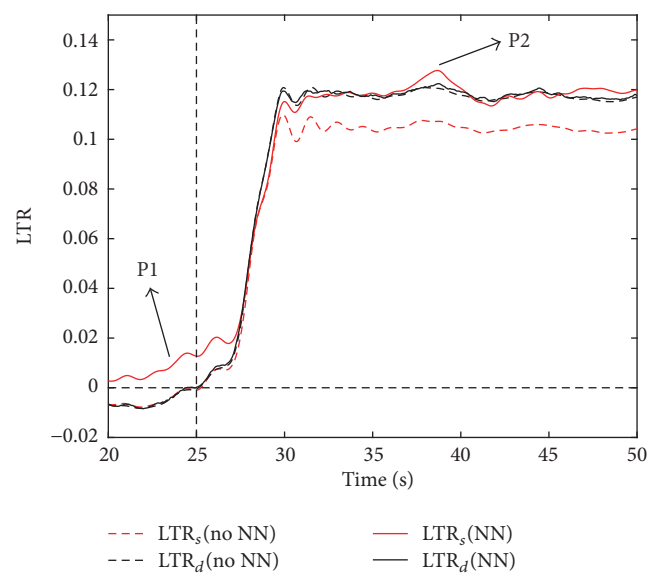

Figure 17: Comparison of different rollover indexes in the ramp test.

NN is bigger than θ without NN as a result of θ_r. Compared with the test results, θ with NN agrees with the test roll angle well when the roll angle is positive but has some errors when the roll angle is negative. In general, θ with NN has a better precision more than θ without NN.

Figure 20 represents the results of different *LTR*s and shows the consistency of their relationship in the ramp test. To analyze snake test in detail, 3 most dangerous moments (P1, P2, P3) are selected to be discussed. The related data are presented in Table 3. In terms of test results, the rollover tendency should be P1 < P2 < P3. The result of LTR$_d$(NN) and LTR$_s$(NN) are right. LTR$_d$ gives P3 < P2 < P1 and LTR$_s$ gives P1 = P3 < P2, which are wrong. Moreover, LTR$_d$(NN) shows bigger differences between these selected moments than LTR$_s$(NN).

4.3. Discussion. For the rollover model, the results of the numerical calculation are satisfying compared with the test data in general. The lateral acceleration of sprung mass is slightly more violent than that of the unsprung mass. The roll angle with neural network optimization is obviously more accurate than that without optimization. When the steering wheel angle δ_{st} is small, the errors of numerical calculation

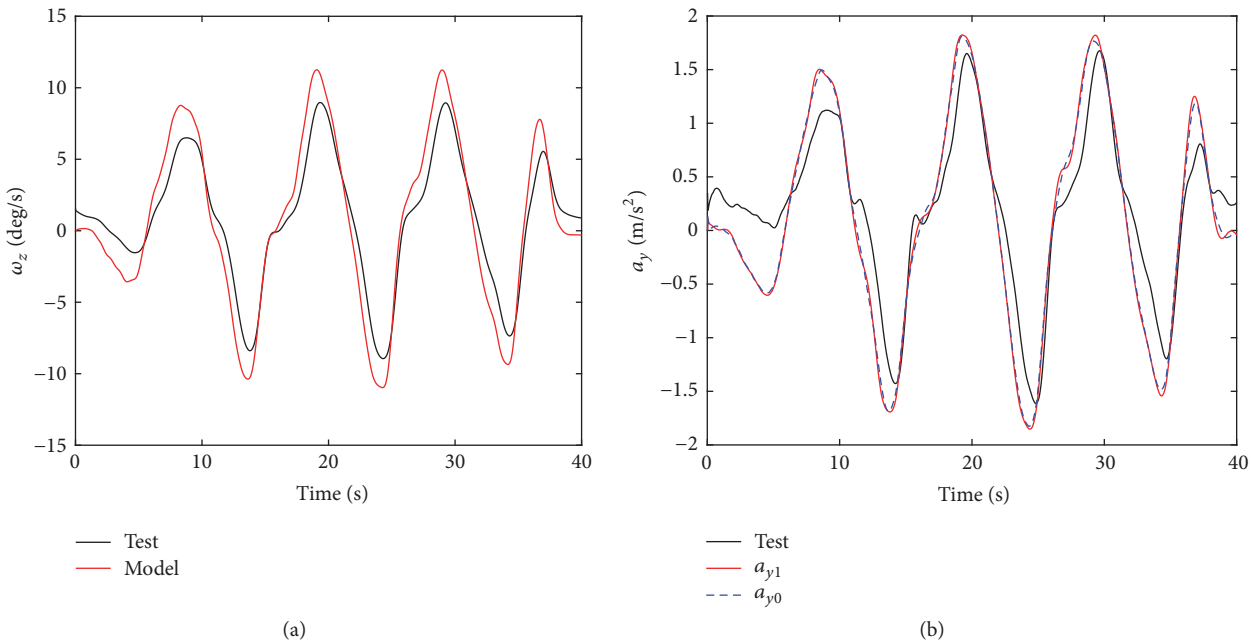

Figure 18: Results of numerical calculation in snake test.

Table 3: Comparison of three peak values of different rollover indexes.

Data	Test θ/°	Test a_y/(m/s^2)	Rollover status	LTR$_d$(NN)	LTR$_d$	LTR$_s$(NN)	LTR$_s$
P1	−1.7	1.63	Least dangerous	−0.173	−0.183	−0.204	−0.209
P2	−1.88	1.67	Medium dangerous	−0.176	−0.189	−0.205	−0.214
P3	4.68	−1.65	Most dangerous	0.196	0.182	0.208	0.209

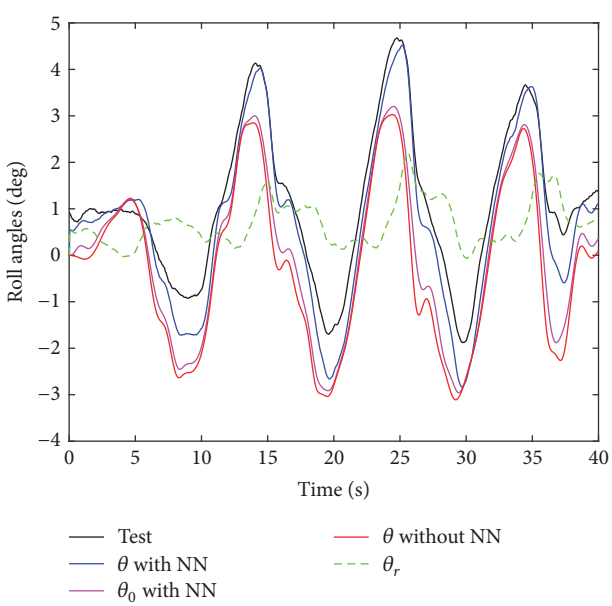

Figure 19: Comparison of different roll angles in snake test.

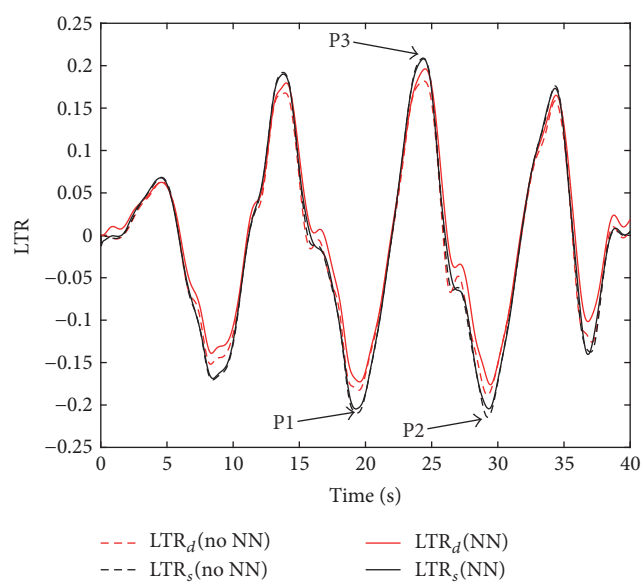

Figure 20: Comparison of different rollover indexes in snake test.

become large. There might be two possibilities: one is that there are empty travels in the steering wheel that cannot be excluded of the measurement instrument, causing the measured value to contain some effortless part; the other one is that the linear assumption for δ_{st} and $\delta_{1,in}$ leads to some inaccuracy.

The BP neural network demonstrates a new way to consider the unknown road inclination angle influence on rollover. Of all the four rollover indexes, the performance of LTR_d(NN) is the best to evaluate the impending rollover on the slope road surface accurately. This suggests that the road inclination angle predicted by the BP network plays an important role in the rollover model. In addition, the improvement brought by BP network of LTR_d is quite greater than that of LTR_s.

5. Conclusion

This paper proposed a new rollover index, based on the dynamic form of *LTR* optimized by the BP neural network. By comparing different rollover indexes with the test result, the sensitivity and practicality of the new rollover index are verified. The conclusion of this paper is summarized as follows:

(1) The nonlinear characteristics of the hydropneumatic suspension are studied, and the formulas of the suspension equivalent stiffness and equivalent damping are given, providing a practical way to describe the nonlinear characteristics of suspension for the rollover model. Based on the Lagrangian second-class equation and Ackerman steering strategy, this paper presents a generalized rollover model considering the road inclination, which has important meaning for studying heavy-duty vehicles.

(2) With the BP neural network, the relationship between the total roll angles and the road inclination is established efficiently. It highly optimizes and improves the accuracy of the rollover model. The improved rollover index with BP network is able to evaluate the impending rollover tendency more accurately.

(3) The BP neural network is proved to be useful for improving the rollover index performance. To train the BP network with efficiency, some measurements including proper learning rate, trying different hidden neurons, and random training samples are encouraged.

Conflicts of Interest

The authors declare that they have no conflicts of interest.

References

[1] D. C. Viano and C. S. Parenteau, "Rollover crash sensing and safety overview," *SAE Technical Papers*, 2004.

[2] K. M. Pollack, N. Yee, M. Canham-Chervak, L. Rossen, K. E. Bachynski, and S. P. Baker, "Narrative text analysis to identify technologies to prevent motor vehicle crashes: Examples from military vehicles," *Journal of Safety Research*, vol. 44, no. 1, pp. 45–49, 2013.

[3] R. L. LeFevre and R. E. Rasmussen, "Manufactures overview of rollover resistance technology," in *Proceedings of the Proceeding 13th International Technical Conference on Experimental Safety Vehicles*, 1991.

[4] *Road Fatality File, Federal Office of Road Safety*, Department of Transport and Communication, Canberra, Australia, 1998.

[5] T. Shim and C. Ghike, "Understanding the limitations of different vehicle models for roll dynamics studies," *Vehicle System Dynamics*, vol. 45, no. 3, pp. 191–216, 2007.

[6] M. P. Czechowicz and G. Mavros, "Analysis of vehicle rollover dynamics using a high-fidelity model," *Vehicle System Dynamics*, vol. 52, no. 5, pp. 608–636, 2014.

[7] G. Andrzej, N. Lu, Z. K. Ldentremont, and S. M. Amp, "An investigation into dynamic measures of vehicle rollover propensity," *Drive System Technique*, 1993.

[8] J. Preston-Thomas and J. H. Woodrooffe. F, "A feasibility study of a rollover warning device for heavy trucks," *Transport Canada Publication*, 1990.

[9] B.-C. Chen and H. Peng, "A real-time rollover threat index for sports utility vehicles," in *Proceedings of the American Control Conference*, pp. 1233–1237, June 1999.

[10] B. C. Chen and H. Peng, "Rollover warning of articulated vehicles based on a time-to-rollover metric," in *Proceedings of the ASME International Mechanical Engineering Conference and Exhibition*, 1999.

[11] B.-C. Chen, "Human-in-the-loop optimization of vehicle dynamics control with rollover prevention," *Vehicle System Dynamics*, vol. 41, pp. 252–261, 2004.

[12] B.-C. Chen and H. Peng, "Differential-braking-based rollover prevention for sport utility vehicles with human-in-the-loop evaluations," *Vehicle System Dynamics*, vol. 36, no. 4-5, pp. 359–389, 2001.

[13] J. Cao, L. Jing, K. Guo, and F. Yu, "Study on integrated control of vehicle yaw and rollover stability using nonlinear prediction model," *Mathematical Problems in Engineering*, vol. 2013, Article ID 643548, 15 pages, 2013.

[14] Z. Yanjun, L. Dequan, and H. Limei, "Rollover warning for school bus based on T-S fuzzy neural network optimized TTR," *Mechanical Design*, vol. 10, pp. 44–49, 2014.

[15] J. Zhao, L. T. Guo, B. Zhu, Q. L. Huang, S. C. Li, and X. Zhou, "Rollover warning for light vehicles based on NN-TTR algorithm," *Journal of Jilin University*, vol. 42, no. 5, pp. 1083–1088, 2012.

[16] G. Phanomchoeng and R. Rajamani, "New rollover index for the detection of tripped and untripped rollovers," *IEEE Transactions on Industrial Electronics*, vol. 60, no. 10, pp. 4726–4736, 2013.

[17] G. Phanomchoeng and R. Rajamani, "Real-time estimation of rollover index for tripped rollovers with a novel unknown input nonlinear observer," *IEEE/ASME Transactions on Mechatronics*, vol. 19, no. 2, pp. 743–754, 2014.

[18] D. Hyun and R. Langari, "Modeling to predict rollover threat of tractor-semitrailers," *Vehicle System Dynamics*, vol. 39, no. 6, pp. 401–414, 2003.

[19] D. R. Woerner, R. Ranganathan, and A. C. Butler, "Developing an artificial neural network for modeling heavy vehicle rollover," *SAE Technical Papers*, 2000.

[20] L. V. Fausett, *Fundamentals of Neural Networks: Architectures, Algorithms, And Applications*, Pearson Schweiz Ag, 1993.

[21] D. E. Rumelhart, G. E. Hinton, and R. J. Williams, "Learning representations by back-propagating errors," *Nature*, vol. 323, no. 6088, pp. 533–536, 1986.

[22] G. Meng, "Analysis of turning characteristic and the principle of Ackerman turning for vehicle," *Mechanical Research Application*, vol. 20, no. 4, pp. 36–38, 2007.

[23] K. Küçük, H. K. Yurt, K. B. Arikan, and H. Imrek, "Modelling and optimisation of an 8 × 8 heavy duty vehicle's hydro-pneumatic suspension system," *International Journal of Vehicle Design*, vol. 71, no. 1, pp. 122–138, 2016.

[24] K. Guo, Y. Chen, Y. Yang, Y. Zhuang, and Y. Jia, "Modeling and simulation of a hydro-pneumatic spring based on internal characteristics," in *Proceedings of the 2011 2nd International Conference on Mechanic Automation and Control Engineering, MACE 2011*, pp. 5910–5915, China, July 2011.

[25] J.-L. Tong, W. Li, and S.-L. Fu, "Effect analysis of main parameters of hydro-pneumatic spring on suspension system performances," *Journal of System Simulation*, vol. 20, no. 9, pp. 2271–2274, 2008.

[26] J. Sun, G. Zhao, and J. Lv, "Simulation and Analysis on Damping Capacity of HPS with Isolated Single-chamber Based on AMESim," *Hydraulics Pneumatics & Seals*, vol. 30, no. 6, pp. 24–27, 2010.

[27] G. Jun, *Artificial Neural Network Theory And Simulation Example*, Mechanical Industry Press, 2007.

[28] C. Zong, Z. Yu, Q. Miao, and B. Zhang, "Research on rollover warning algorithm of heavy commercial vehicle based on prediction model," in *Proceedings of the 2010 International Conference on Computer, Mechatronics, Control and Electronic Engineering, CMCE 2010*, pp. 432–435, chn, August 2010.

[29] P. Gaspar, I. Szaszi, and J. Bokor, "Reconfigurable control structure to prevent the rollover of heavy vehicles," *Control Engineering Practice*, vol. 13, no. 6, pp. 699–711, 2005.

[30] P. Gaspar, I. Szaszi, and J. Bokor, "The design of a combined control structure to prevent the rollover of heavy vehicles," *European Journal of Control*, vol. 10, no. 2, pp. 148–162, 2004.

[31] D. J. M. Sampson and D. Cebon, "Active roll control of single unit heavy road vehicles," *Vehicle System Dynamics*, vol. 40, no. 4, pp. 229–270, 2003.

[32] A. J. P. Miege and D. Cebon, "Optimal roll control of an articulated vehicle: Theory and model validation," *Vehicle System Dynamics*, vol. 43, no. 12, pp. 867–884, 2005.